Geofluids (2005) **5**, 140–150

Evolution of fluid chemistry during travertine formation in the Troll thermal springs, Svalbard, Norway

Ø. HAMMER[1], B. JAMTVEIT[1], L. G. BENNING[2] AND D. K. DYSTHE[1]

[1]*PGP – Physics of Geological Processes, University of Oslo, Oslo, Norway;* [2]*School of Earth Sciences, Earth and Biosphere Institute, University of Leeds, Leeds, UK*

ABSTRACT

Arctic hydrothermal springs at Bockfjorden, Svalbard, have isotope and trace element signatures indicative of derivation from glacial melt waters with minor contribution from seawater. Downstream gradients in water chemistry, isotopic composition and carbonate precipitation rates have been documented for the Troll spring and travertine terrace system. The main controls on the downstream evolution of these parameters are carbon dioxide degassing, calcite precipitation, evaporation and biological activity. The carbonate precipitation rates not only show an approximately parabolic dependence on the calcite supersaturation levels, but depend also on local hydrodynamics. Downstream loss of light isotopes of oxygen and hydrogen can be explained as an effect of evaporation, as estimated using chloride as a conservative marker. Biological activity affects nitrate and bromide concentrations and influences the morphology of calcite precipitates.

Key words: arctic hot springs, carbonate precipitation, fluid evolution, travertine

Received 10 May 2004; accepted 11 November 2004

Corresponding author: Øyvind Hammer, PGP – Physics of Geological Processes, PO Box 1048 Blindern, 0316 Oslo, Norway.
Email: ohammer@nhm.uio.no. Tel: +47 22 85 66 26, Fax: +47 22 85 51 01.

Geofluids (2005) **5**, 140–150

INTRODUCTION

The Troll and Jotun thermal spring complexes at Bockfjorden, Svalbard (Hoel & Holtedahl 1911; Banks *et al.* 1998), are the northernmost documented hot springs on land, with the Troll springs situated at 79°23′N, 13°26′E (Fig. 1). The temperature of the spring waters is moderate, with 28.3°C as the highest recorded value (Hoel & Holtedahl 1911). The temperatures at the sources are remarkably stable through the year, and the springs remain ice-free throughout winter (J. Heldmann, personal communication). These springs are situated along a major fault line, in the vicinity of volcanoes that may have been active as recently as the Pleistocene (Skjelkvåle *et al.* 1989). Banks *et al.* (1998) characterized the water chemistry of the main springs in detail, and found that the Troll springs are supplied with sodium and bicarbonate-rich waters. They suggested that the waters originate from a deep reservoir of thermal, probably fossil, seawater modified by water–rock interaction and dilution with considerable amounts of cold groundwater.

Both the Troll and Jotun springs deposit calcium carbonate in the form of calcite, with the source presumably in the underlying Proterozoic marble of the Generalfjellet Formation. Several of the Troll springs have produced spectacular travertine rimstone and terrace morphologies. The 3A spring system in the Troll Spring area (nomenclature from Banks *et al.* 1998) is associated with a terraced area around 100 m across, although only the topmost pools are presently filled with water (Fig. 2). We visited Bockfjord in August 2003, and briefly in August 2004, with the purpose of studying travertine geomorphology and pattern formation, as well as carbonate precipitation processes and the spatial distribution of chemical parameters within the Troll 3A spring.

In other springs around the world, it is believed that travertine precipitation is mainly driven by CO_2 degassing (Buhmann & Dreybrodt 1985; Dreybrodt *et al.* 1992; Fouke *et al.* 2000; Lu *et al.* 2000). When the water first comes in contact with the atmosphere it is typically somewhat acidic, due to high concentrations of carbon dioxide. As the water moves downstream carbon dioxide is

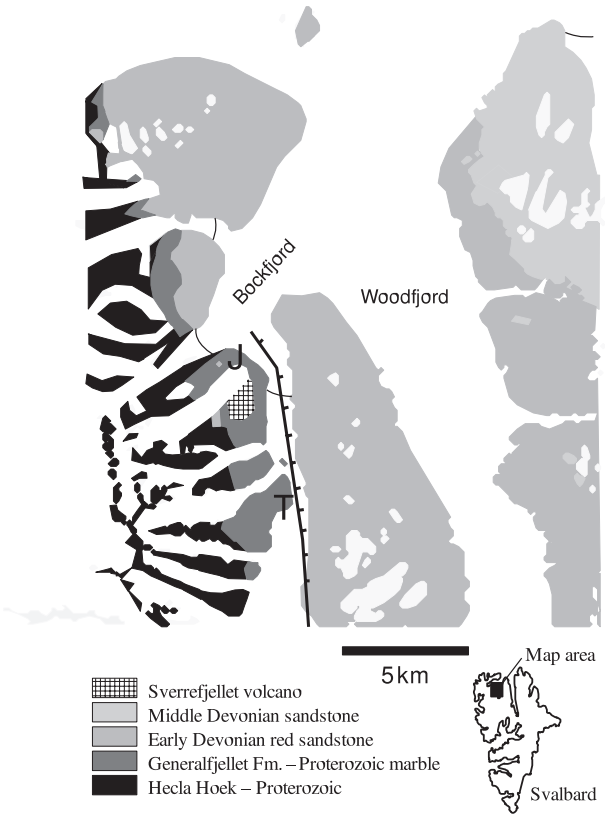

Fig. 1. Sketch of the Bockfjorden area, with the Troll (T) and Jotun (J) springs. White areas on land are glaciers, moraine or sandur.

Fig. 2. Aerial photograph of the Troll 3A travertine terrace system, about 100 m across. Source in the upper left of the picture (arrow). Only the uppermost terraces are currently filled with water.

progressively lost to the atmosphere, increasing the pH and consequently the calcium carbonate supersaturation levels. By mapping local variations in water chemistry within the Troll 3A spring, we can clearly document such trends, as well as the effects of water evaporation and the influence of biological activity in the pools.

METHODS

Field procedures

The geometry of the Troll 3A pools filled with water in 2003, and the positions of the fluid sampling points as well as the placement points for the experimental slabs and slides were determined using a Leica TCRA1103 total station (theodolite and laser ranging device). These sampling and deployment points are shown in Fig. 3.

Temperatures were measured with a digital thermometer to a precision of 0.05°C. A Hanna Instruments HI 9025 pH meter that was calibrated in the field with pH 7.00 and 10.01 buffer solutions (0.05 log units) was used for *in situ* pH measurements. Similarly, conductivity was measured in the field with a Hanna Instruments HI 7031 conductivity meter (0.02 mS cm^{-1}).

Water samples for chemical analyses were collected close to the surface of the Troll 3A pools at each sampling point (Fig. 3) by filling acid-washed plastic bottles to the rim to avoid degassing. In addition, several upstream and downstream fluid samples from the main springs as well as a cold spring sample (corresponding to sample K1 of Banks *et al.* 1998) were collected for isotopic analyses. Calcium concentrations were measured immediately in the field using an Aquamerck calcium test kit (Merck). Carbon dioxide concentrations were also measured in the field using a Hach digital titrator kit. Alkalinity, calcium and total hardness were measured on board of the expedition ship about 6 h after sampling (bottles were filled to the rim to prevent degassing), using Hach digital titrator kits. The calcium values measured in this way were consistently around 10% lower than those measured in the field. This was probably a consequence of the slow equilibration reactions in the field caused by the lower temperatures. Alkalinity values were in general agreement with a smaller number of control titrations made in the field.

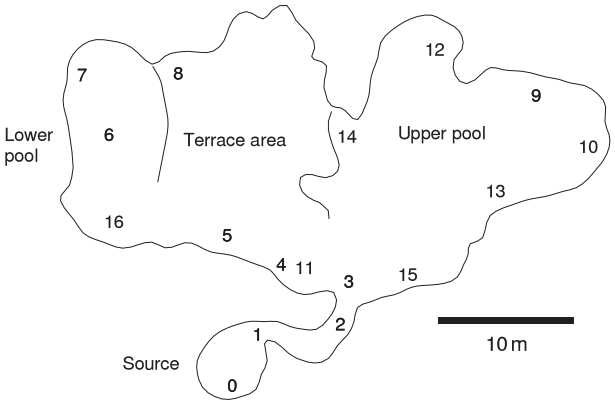

Fig. 3. Map of wet areas within the Troll 3A spring, with sample positions.

In order to estimate carbonate precipitation rates the method of Zaihua *et al.* (1995) was used. Ten limestone slabs ($4 \times 2 \times 0.5$ cm) were polished, washed in ethanol and dried for 24 h at 60°C before weighing on a digital scale. The slabs were submersed in the travertine pools for 73 h, and kept clear of the bottom by metal clips. Furthermore, ethanol-cleaned microscope slides were placed at two points in the pools (points 11 and 12, Fig. 3) in such a way that the slides were either fully submerged or were sticking out above the water–air interface by about 5 mm.

All measurements reported here were taken during our visit in August 2003. When re-visiting the site in August 2004, we found that the water had found a new route from the upper pool, possibly because of travertine precipitation. As a result of this, the lower pools from 2003 had become stagnant, while other old, previously dry pools had been reactivated.

Laboratory measurements

Anion concentrations were measured in filtered water samples (Whatman 0.45 μm polycarbonate filters) using ion chromatography (IC, precision RSD <5%), while cations were determined from acidified samples (HNO_3) using inductively coupled plasma-mass spectrometry (ICP-MS) at the Department of Earth Sciences, University of Leeds (precision RSD <3%).

Stable isotope compositions were measured from separate aliquots of the water samples at the Bjerknes Centre, University of Bergen ($\delta^{18}O$ and $\delta^{13}C$) and at the Southampton Oceanography Institute (δD). Reported precisions were <0.1‰ (O and C) and <1% (D). Oxygen and hydrogen values are reported relative to the SMOW standard, and carbon relative to PDB.

The deployed limestone slabs were retrieved after 73 h and stored in centrifuge tubes. Back in the laboratory, the slabs were washed thoroughly in ethanol, dried for 24 h and weighed, to a precision of ±0.05 mg. The weight increase (precision ±0.1 mg; control slabs showed zero weight gain) was used to calculate the precipitation rate following the method of Zaihua *et al.* (1995). The weighing precision provides an expected precision of ±0.002 mg cm^{-2} day^{-1} for the reported precipitation rates. The newly formed precipitates on selected slabs were imaged using scanning electron microscopy (SEM, 15–20 kV) after gold coating.

Similarly, selected microscope slides were retrieved after 70 h and stored in centrifuge tubes until analysis. The formed precipitates were characterized using a field-emission scanning electron microscope (FEG-SEM, LEO 1530). The slides were deposited on stubs, air-dried, coated with a 3-nm palladium layer and examined at 1–3 keV at a working distance of 2–4 mm using an in-lens secondary electron detector.

RESULTS

Source fluid characteristics

The oxygen and hydrogen isotopic ratios for a number of upstream and downstream samples in the Troll hydrothermal springs 1A, 2A and 3A are shown in Fig. 4. The values follow a downstream trend away from the meteoric line, as an effect of evaporation (see below). The oxygen isotopic composition at the source is ca. −17.5‰. A sample from a nearby cold spring is shown for comparison, displaying less negative isotopic ratios (−15.8‰ $\delta^{18}O$). Ice core records from the Lomonosovfonna glacier at 78°44′N, 17°34′E, 1020 m above sea level, show a mean $\delta^{18}O$ value of −15.7‰ from the period 1920 to 1997 (Isaksson *et al.* 2001), in good accordance with the Troll cold spring value. Similarly, the average $\delta^{18}O$ ice core value at

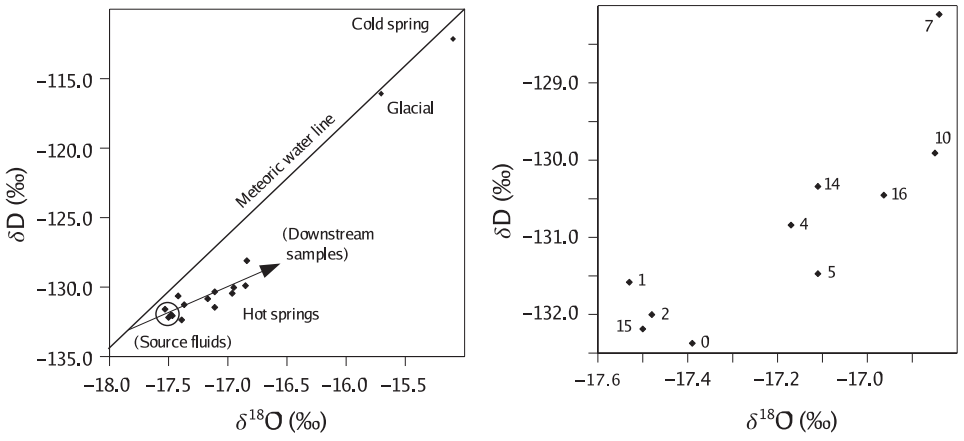

Fig. 4. Oxygen versus hydrogen isotopic ratios. Left: all samples from the Troll hot springs 1A, 2A and 3A, and the Troll cold spring. The 'Glacial' point represents the 1920–97 average from the Lomonosovfonna ice core (Isaksson *et al.* 2001). Right: close-up of the samples within spring 3A, with sample numbers as given in Fig. 3.

Austfonna, Nordaustlandet, further to the east in Svalbard (750 m above sea level), is −16.7‰ for the period from 1900 to 2000, while the average from 1400 to 1900 is −18.7‰ (Watanabe *et al.* 2001). We conclude from this that the Troll cold spring is sourced from relatively recent surface waters. Assuming that the source for the hot spring fluids is predominantly groundwater, mainly derived from the close upland glaciers, the isotopic data indicate a source of more ancient origin, at least before 1900. Most likely, these melt waters derive from snow precipitated at somewhat lower altitudes than those of Lomonosovfonna and Austfonna, and are therefore expected to show less negative $\delta^{18}O$ values for equal ages (e.g. Poage & Chamberlain 2001).

There are no systematic changes in the $\delta^{13}C$ composition from source to sink in the pool. $\delta^{13}C$ values of spring waters scatter around −1‰, broadly consistent with carbon derivation from dissolved marine carbonates (marbles) at depth.

The elevated salinity of the spring water (but below 1 ppt) is most likely mainly due to seawater influx (Banks *et al.* 1998). The Br concentration at the source of the Troll 3A spring is 0.89 mg l^{-1}. Using a typical seawater Br concentration of 65 mg l^{-1}, and assuming that Br behaved as an inert species at depth, this indicates an amount of seawater corresponding to about 1.4% in the Troll fluids.

Na/Br and Cl/Br ratios for the Troll hot springs are shown in Fig. 5. The fluids are relatively enriched in Na and depleted in Cl relative to seawater, most likely as a result of water–rock interactions modifying the meteoric-seawater mix. A gain in Na and a drop in Cl relative to seawater are expected from reactions involving feldspar dissolution and growth of sheet silicates at depth. The linear trend through the origin is most easily explained by removal of Br within the pools (see below).

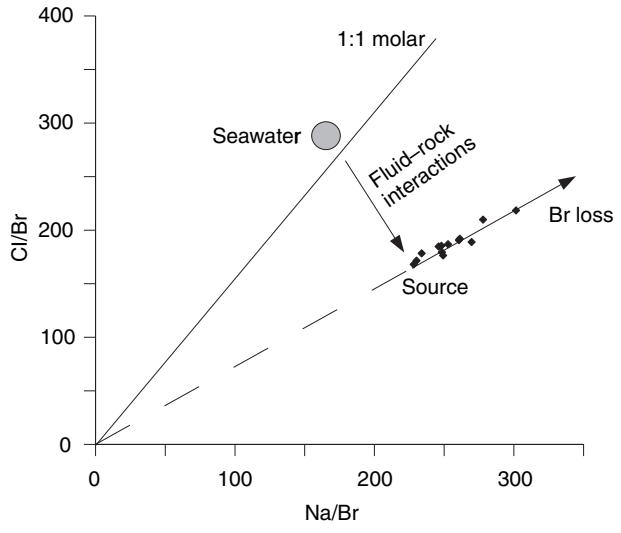

Fig. 5. Na/Br and Cl/Br mass ratios for samples within the Troll 3A spring complex.

Downstream water chemistry in the Troll 3A spring

The hydrochemical parameters at different sampling points (Fig. 3) are shown in Tables 1 and 2, and are portrayed graphically in Figs 6 and 7. The contour maps of Fig. 6 are of course relatively unconstrained due to the small number of sampling points, but are still useful for visualization and show a consistent downstream trend for most parameters.

Temperature drops from an initial 27.4°C at the source down to 13.9°C at the most distal sampling point in the travertine pools (Fig. 6B). The air temperature varied between 8.6 and 14.9°C in the 24 h before measurement. Banks *et al.* (1998) measured 25.6°C at their sampling point 3A1 (exact position within spring 3A not given).

Although the gas composition was not measured, visible gas bubbling in the source most probably involves CO_2 degassing, although the smell of H_2S was also noticeable. Dissolved carbon dioxide was measured only at selected locations, partly because sampling without strong agitation was difficult in shallow water (Table 1). Nevertheless, the systematic downstream removal of CO_2 is obvious (Fig. 6D), and <40% of the original concentration is retained at the most distal location. As carbon dioxide was measured with an acidity titration method, it is not surprising that there is a strong downstream increase in pH, from an initial 6.58 at the source up to 8.41 at the most distal sampling point 8 (Figs 6C and 7A). Banks *et al.* (1998) measured a pH of 6.83 at their sampling point 3A1, corresponding to our value between sampling points 2 and 3.

The concentration of dissolved calcium decreases from 110 mg l^{-1} at the source down to 70–90 mg l^{-1} at distal sampling points (ICP-MS values; Figs 6E and 7B). Banks *et al.* (1998) and also Hoel & Holtedahl (1911) similarly reported a calcium concentration of 110 mg l^{-1}.

Our values for alkalinity (478–579 mg l^{-1}) are slightly lower than those measured by Banks *et al.* (1998), who reported 13.1 mEq l^{-1} (655 mg l^{-1} as $CaCO_3$). This may be a consequence of the manual titration method employed in the field. In fact, the charge balance as calculated from ICP-MS, IC, pH and titrated alkalinity shows a negative charge balance error of up to 8.5% (in sample 7). This error virtually disappears when using the higher alkalinity values of Banks *et al.* (1998). We therefore assume that our alkalinity values are somewhat too low, but the presented downstream trends are still valid.

Ba and Sr concentrations correlate positively with Ca (Fig. 7) and show a decrease by ca. 10% from the spring source to the terrace rims. The trends in Fig. 7 can be used to constrain the partitioning of these elements

Table 1 Field measurements from the Troll 3A spring.

Sample	*T*	pH	Ca^{2+} (mg l^{-1})	CO_2 (mg l^{-1})	Alk (mg l^{-1})	TH	EC (mS cm^{-1})	Precipitation	SI
0	27.4	6.58	134	372	579	163	1.74		−0.2
1	27.0	6.70	133	330	560	154	1.72	0.00	−0.1
2	27.1	6.70	122		558	154	1.73	−0.01	−0.1
3	25.9	7.01	112		562	148	1.70	0.00	0.2
4	23.1	7.75	116	286	572	286	1.69	0.16	0.9
5	18.6	7.90	112	228	484	110	1.46	0.72	1.0
6	14.6	8.36	96		500	96	1.58	0.25	1.4
7	14.2	8.37	100	140	498	107	1.34	1.26	1.4
8	13.9	8.41	90		484	98	1.57	1.30	1.4
9	14.7	8.26	110		498	111	1.61	0.65	1.3
10	16.2	8.24	100		478	110	1.60	0.32	1.2
11	23.2	7.66	116	320	564	153	1.67		0.8
12	14.8	8.28	103	262	502	106	1.36		1.3
13	14.4	8.17							

Alk, alkalinity; TH, total hardness; SI saturation index. Alkalinity is given in units of mg l^{-1} as $CaCO_3$. Carbonate precipitation rate in mg cm^{-2} day^{-1}. Log-transformed SI calculated using ICP-MS values for calcium.

Table 2 Laboratory analysis (isotopic, ICP-MS and IC) of water samples.

Sample	$\delta^{18}O$	δD	Ca^{2+}	Mg^{2+}	Na^{+}	Si^{4+}	Ba^{2+}	Sr^{2+}	Cl^{-}	Br^{-}	SO_4^{2-}	NO_3^{-}
0	−17.39	−132.37	109.90	33.07	203.1	18.5	0.153	1.154	149.66	0.89	60.51	0.07
1	−17.53	−131.58	109.40	32.25	199.3	17.9	0.152	1.130	149.70	0.81	60.20	0.20
2	−17.48	−132.00	114.90	33.29	203.3	18.2	0.159	1.167	148.81	0.78	59.76	0.18
4	−17.17	−130.84	90.13	32.01	200.1	18.2	0.144	1.138	151.12	0.72	64.10	0.10
5	−17.11	−131.47	93.30	33.18	204.8	18.6	0.149	1.165	151.42	0.81	60.39	0.21
7	−16.84	−128.11	84.30	34.30	208.7	19.4	0.168	1.090	139.34		31.72	
10	−16.85	−129.91	72.05	33.31	207.2	18.3	0.131	1.097	154.46	0.90	61.92	0.15
11			105.20	33.31	205.9	18.3	0.146	1.139	158.72	0.68	62.04	0.23
12			86.37	34.92	217.7	19.0	0.134	1.129	157.55	0.65	62.81	0.18
14	−17.11	−130.34	79.07	32.85	205.9	19.3	0.136	1.106	153.94	0.83	61.15	0.14
15	−17.50	−132.18	103.30	34.73	215.8	19.2	0.157	1.208	151.20	0.80	60.52	0.31
16	−16.96	−130.45	69.71	32.89	205.1	18.9	0.133	1.057	148.56	0.68	58.99	0.19

Oxygen and hydrogen isotope ratios are relative to SMOW. Ion concentrations are in mg l^{-1}.

between the spring water and the precipitating carbonates along the flow path (see below).

Calcite saturation indices (SI) are given as the log ratio of the calcite ion activity product to the solubility product of calcite. Calcium concentrations were taken from the ICP-MS data, while carbonate concentrations were estimated from pH and titrated alkalinity. Activities were corrected using the measured ionic strengths (conductivities). SIs as given here were calculated by hand. Using the computer program PHREEQC version 2, Parkhurst & Appelo (1999) produced comparable results, except for a very slight (<0.05 log units) reduction in calcite SI values due to the inclusion of Mg in the calculations. The log calcite SI is within 0.2 units from zero in samples 0–3, confirming that the water is saturated with respect to calcite in the 3A spring (Banks *et al.* 1998). In sample 4 the SI has a value of 0.9, increasing up to a maximum of 1.4 in samples 6–9. Increasing alkalinities to the levels measured by Banks *et al.* (1998) raises SI by up to 0.1 log units.

Conductivity (ionic strength) decreases downstream, from 1.7–1.8 mS cm^{-1} in the upstream samples to 1.3–1.6 mS cm^{-1} in the distal samples. Banks *et al.* (1997) reported a conductivity of 16.3 mS cm^{-1}, which seems to be too high by a factor of 10.

The weight increases on the limestone slabs are shown in Table 1. There was no precipitation at sample points 1–3. This is consistent with the near-absence of travertine in this region above the first travertine pool, and provides a check on the accuracy of measurements. The lack of calcium carbonate precipitation is associated with pH values below 7.0. Precipitation rates increase systematically downstream (Fig. 6J). SEM images of the retrieved slabs confirmed that the weight increase (up to 70.4 mg) was mainly due to calcite precipitation. Figure 8A shows an SEM micrograph of limestone sample 1 (source) with no visible precipitation but signs of weak dissolution, while Fig. 8B–D presents precipitates on the most distal sample 7 showing a rich population of calcite crystals.

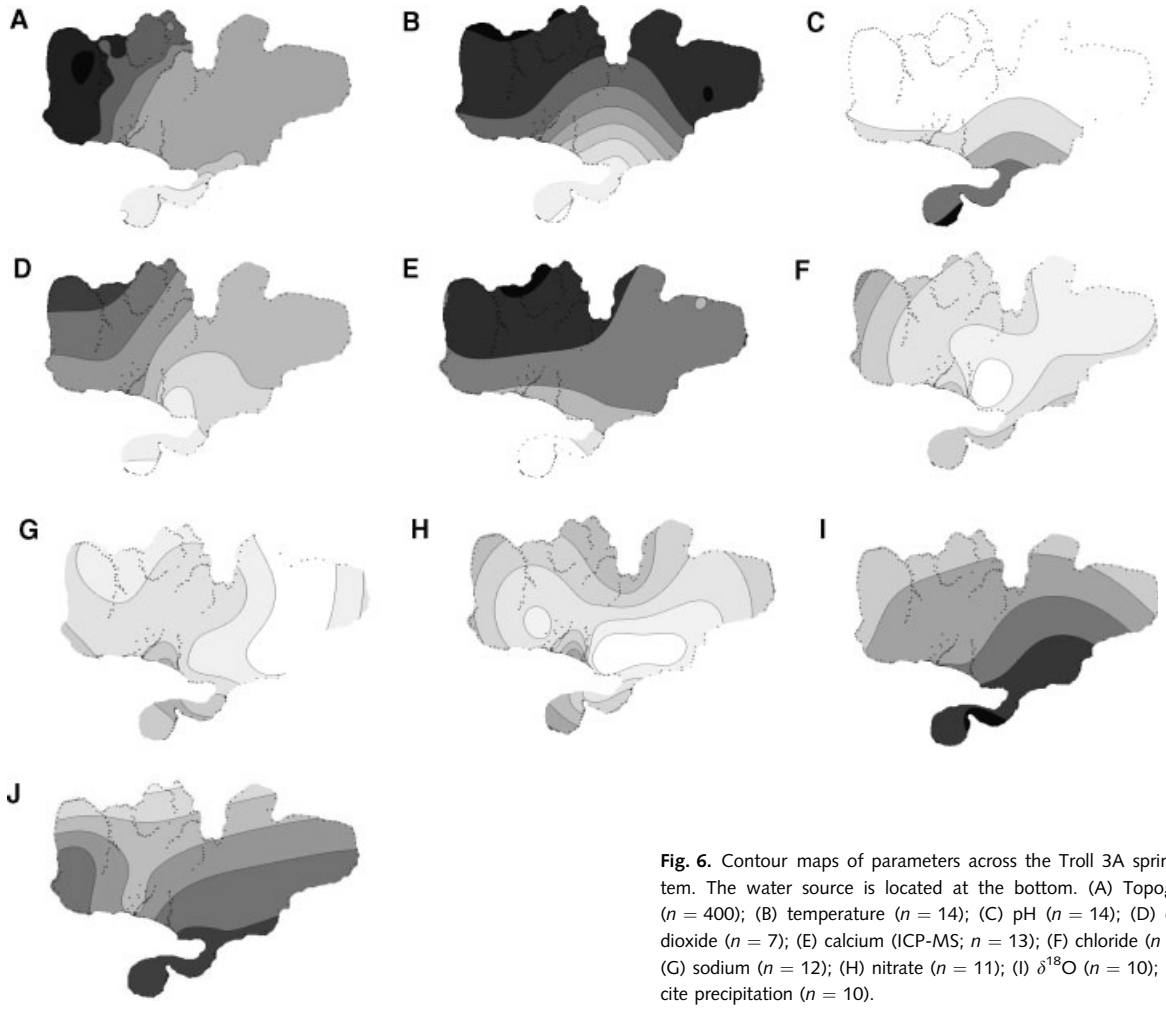

Fig. 6. Contour maps of parameters across the Troll 3A spring system. The water source is located at the bottom. (A) Topography ($n = 400$); (B) temperature ($n = 14$); (C) pH ($n = 14$); (D) carbon dioxide ($n = 7$); (E) calcium (ICP-MS; $n = 13$); (F) chloride ($n = 12$); (G) sodium ($n = 12$); (H) nitrate ($n = 11$); (I) $\delta^{18}O$ ($n = 10$); (J) calcite precipitation ($n = 10$).

On all deployed microscope slides the newly formed precipitates were well-crystalline, single or aggregated euhedral calcites either of pinacoidal, rhombohedral or hexagonal habit. The morphologies and distribution/aggregation patterns on the slides depended on the deployment mode. When the slides were fully immersed in the pool, usually single well-crystalline habits with smooth surfaces formed at times (Fig. 9A,B). When the slides were immersed with part of the slide protruding above the water–air interface, the resulting precipitates developed aggregates and clusters primarily on the slide edge (Fig. 9C). The rate of growth on the slide edge was much faster than when the slides were fully immersed. When compared with the deployed limestone slabs, the crystal habits of the newly formed precipitates were substantially different (compare Figs 8B,C and 9A–C), and although a quantification of the growth rates on the slides was not possible, the microscopic observations of calcite precipitated on the slides support those from the slabs.

To elucidate the role micro-organisms have on calcite precipitation rates and habits, a piece of the travertine mat from the edge of the pool (point 14, Fig. 3) was also imaged. In the presence of bacterial mats that colonized the newly formed travertine sinters the morphology of the calcite changes, forming much smoother and rounded calcite aggregates (Fig. 9D) intercalated with microbial filaments and diatoms (Fig. 9E,F).

DISCUSSION

The consistent downstream temperature drop indicates that there is little or no addition of hydrothermal water from the ground below the pools, and that the primary fluid source is the spring above the pools.

The downstream increase in pH is directly connected with the loss of carbon dioxide. It is reasonable to assume that much of this loss is due to degassing, although biological removal may also play a part (see the discussion in Fouke *et al.* 2000). It is of interest to note the excellent congruency between the spatial distributions of temperature and pH (Fig. 6B,C). As loss of heat and inorganic loss of carbon dioxide to the atmosphere are controlled by

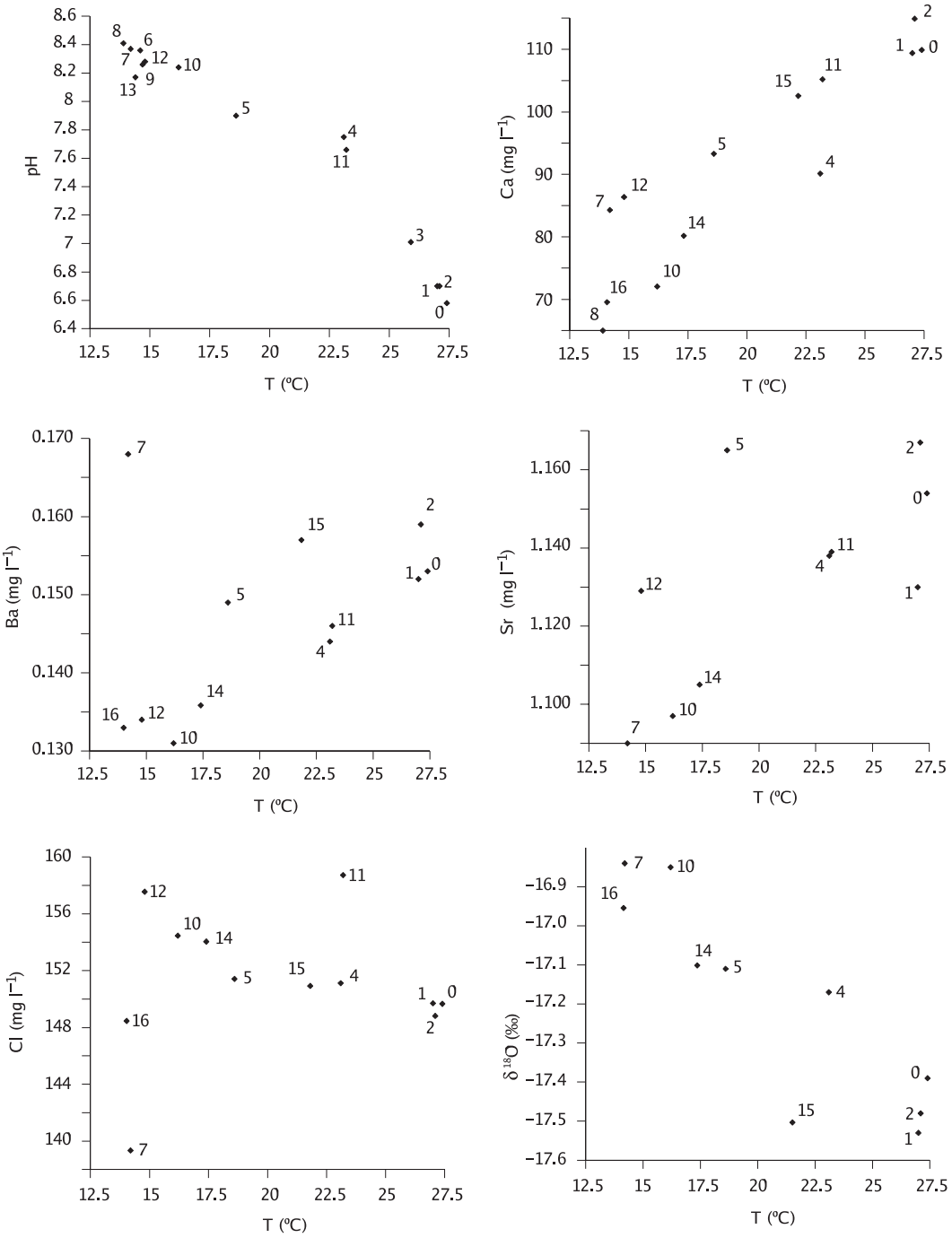

Fig. 7. Scatterplots of parameters versus temperature. Ion concentrations are in mg l^{-1}. Sample positions are as shown in Fig. 4.

analogous physical processes (fluid dynamics, advection and diffusion), this pattern strengthens the case for outgassing rather than biological removal being the dominating process. Micro-organisms are present in the sinters, but the bacteria seem to colonize the precipitates and therefore influence the calcite crystal morphology only once an initial sinter surface has formed, while the diatom frustules most likely represent dead specimens (Fig. 9E,F). The increase in pH produces a progressive oversaturation of calcium carbonate, leading to precipitation of travertine. Correspondingly, the concentration of dissolved calcium decreases downstream.

The systematic downstream reduction in alkalinity can be explained by calcium carbonate precipitation from sampling point 4 and below. Alkalinity stays relatively constant in samples 0–3, but then drops in the more distal

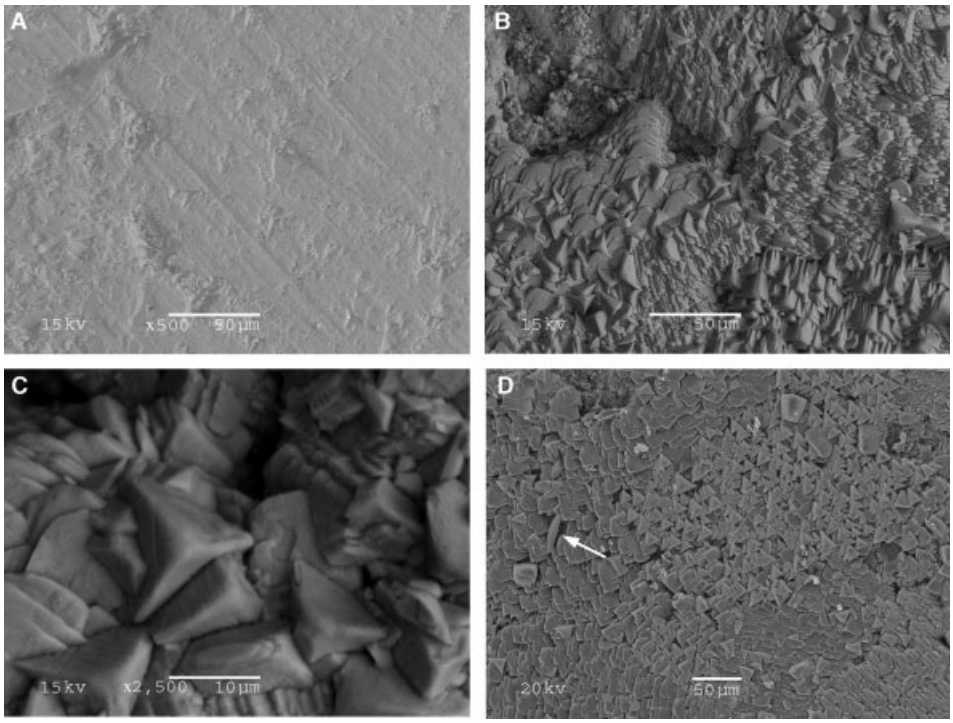

Fig. 8. SEM pictures of limestone slabs after 73-h immersion in the Troll 3A spring. (A) Sample 1, placed close to water source at supersaturation index SI = −0.1. Triangular features are interpreted as shallow etch pits. (B) Sample 7, close to rim in the most distant pool (SI = 1.4). There is considerable build-up of calcite crystals of different habits. (C) Detail of (B). (D) Another region of sample 7, with different crystallization domains. A pennate diatom frustule is embedded into the surface (arrow).

samples. The reduction in alkalinity from the average in upstream samples 0–3 to the average in downstream samples 7, 10 and 12 is 72.1 mg l^{-1} alkalinity as $CaCO_3$, or 28.9 mg l^{-1} as Ca^{2+}. This fits well with the measured reduction in calcium (30.5 mg l^{-1}), indicating that the reduction in alkalinity is mainly due to the precipitation of calcium carbonate. As ions are removed from solution, conductivity (ionic strength) decreases downstream.

The Ba and Sr data portrayed in Fig. 7 can be used to estimate the average partition coefficient between fluid and precipitated carbonate between any pair of sampling points A and B along the fluid flow path. The assumption is that all Ca lost from solution in the same interval is consumed by calcite precipitation. Simple mass balance calculation gives:

$$D_{Sr} = \frac{([Sr^{2+}]_A - [Sr^{2+}]_B)/([Ca^{2+}]_A - [Ca^{2+}]_B)}{([Sr^{2+}]_A + [Sr^{2+}]_B)/([Ca^{2+}]_A + [Ca^{2+}]_B)}.$$

Average D-values across the upper pools from fluid source to terrace margin (points 2–10) are $D_{Ba} = 0.42$ and $D_{Sr} = 0.13$. The strontium value is broadly consistent with the partition coefficients measured at relatively high supersaturation ($\log \Omega > 1$) and precipitation rates $R >$ 2 nmol mg^{-1} min^{-1} (cf. Tesoriero & Pankow 1996). Supersaturation levels between point 2 and 10 in the Troll 3A pool varies from near zero to $\log \Omega = 1.2$ (Fig. 10). The Ba value is however about one order of magnitude higher than expected for calcite precipitation at similar rates (Tesoriero & Pankow 1996). The reason for such high values is not known, but any precipitation of aragonite, which has been observed in the sinters that form in the presence of bacteria, would increase the compatibility of both Ba and Sr in the carbonate precipitate.

The mass of precipitates on the limestone slabs increases systematically downstream, correlating well with pH. The precipitation rate increases quadratically with the degree of supersaturation (Fig. 10), with two major exceptions: precipitation is anomalously high at sample 5, in a region of shallow water and particularly fast flow, and anomalously low at sample 6, which is the only deep-water sample and also in a region of stagnant flow. The highest precipitation rates are measured in the shallow, distal regions of the pools, where flow rates are low due to lack of outflow (water is removed through diffuse infiltration) but the supersaturation is very high. These data therefore indicate that precipitation rates are controlled by a combination of overall water chemistry driven by the gradual removal of CO_2, and local hydrodynamics (Zaihua *et al.* 1995).

We refrain from inferring any particular regime of growth kinetics from the quadratic form of the saturation/precipitation curve, as this curve will be heavily influenced

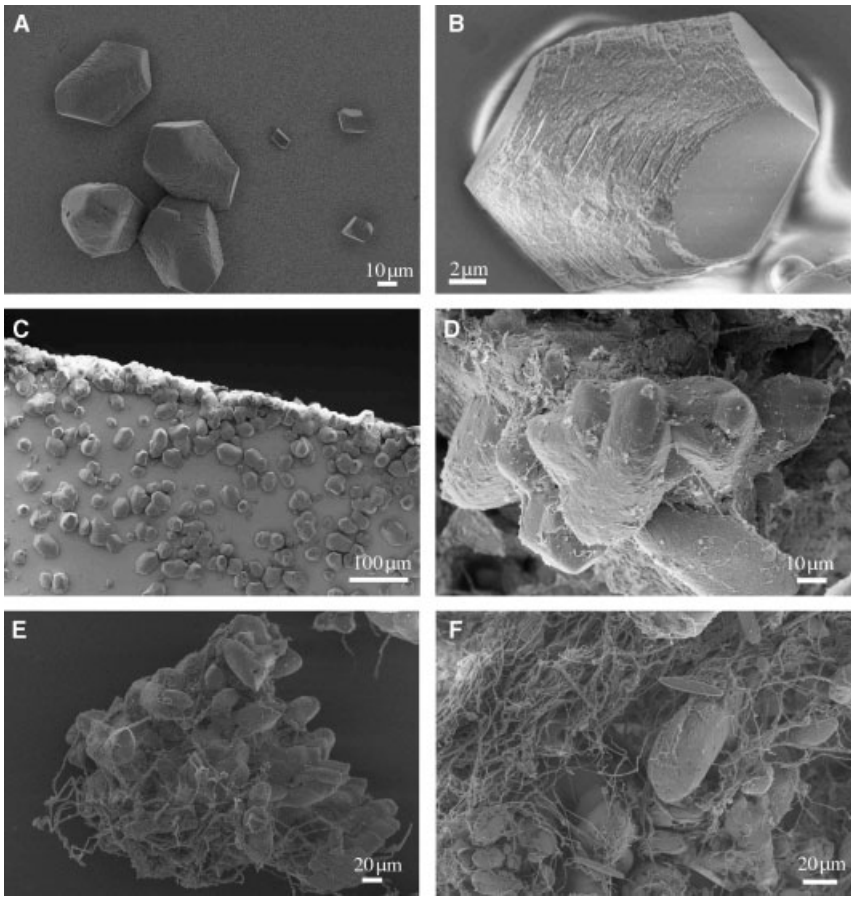

Fig. 9. FEG-SEM microphotographs of newly formed calcite habits that have grown on microscope slides. (A) Slide fully immersed at position 11 shows well-developed calcite crystals mostly as singular grains on the slide (bar = 10 μm). (B) High magnification micrograph of a singular calcite crystal showing the smooth crystal edges (bar = 2 μm). (C) Calcite crystals grown at the top of the slide at the water–air interface; note the habits are similar to the singular slides grown under water but here aggregates of crystals cover the whole slide edge (bar = 100 μm). (D) Calcite crystals grown in the sinter mats at the edge of the pool; note the much more rounded and fuzzy shape of the resulting crystals (bar = 10 μm). (E) Intercalated filamentous bacteria and rounded calcite crystals from a mat at the edge of the pool (bar = 20 μm). (F) Dense filamentous microbial colony and a diatom that are entwined with calcite aggregates grown at the sinter edge (bar = 20 μm).

by the large differences in slab surface area generated during crystal growth.

The highest precipitation rate was 1.30 mg cm^{-2} day^{-1}, or 475 mg cm^{-2} $year^{-1}$, measured at sample point 8 at around 2 cm depth close to the terrace edge but inside the pool. Assuming a density of fresh travertine of roughly 2.5 g cm^{-3}, this indicates a precipitation rate of around 2 mm $year^{-1}$. However, there is reason to believe that precipitation would be much faster than this on the top and outside of terrace edges, where we were not able to measure precipitation rates.

Effects of evaporation

In contrast to the downstream reduction in Ca and alkalinity resulting from precipitation of carbonate, the concentrations of Na, Cl, Mg and sulphate are highest in the large, stagnant uppermost pool. We interpret this as an effect of evaporation. The ratio of Cl between stagnant backwater pool (sample 10) and source is 1.032, the corresponding ratio for Na is 1.020 and for sulphate 1.023. This corresponds to 2–3% evaporation. Relatively strong wind and high temperatures during the period of field observation, low flow rates and the large surface to volume ratio in the water bodies in the pools are all factors that would contribute to this effect.

The $^{18}O/^{16}O$ ratio shows a clear trend of downstream increase (Fig. 6I), correlating well with the chemical parameters connected with carbonate precipitation. However, such an increase in the oxygen isotopic ratio has been assumed to be linked to water evaporation rather than CO_2 degassing and carbonate precipitation (Fouke *et al.* 2000).

At a location L, the ratio between evaporation E and inflow I is given in terms of the isotopic compositions as

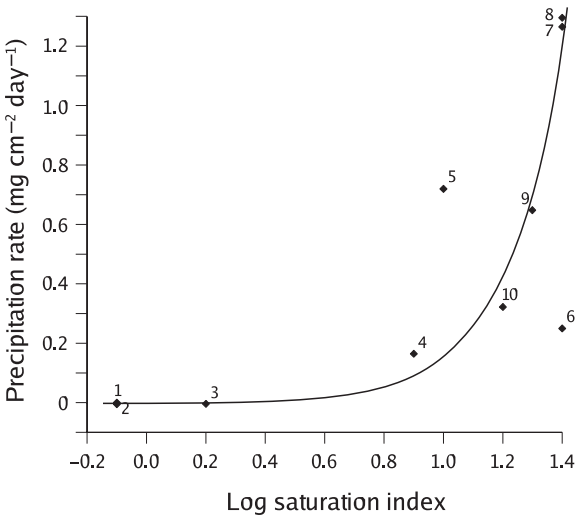

Fig. 10. Calcium carbonate saturation index (log) versus precipitation rate for 10 samples within the Troll 3A spring. Carbonate precipitation rate in mg cm^{-2} day^{-1}. The log-parabolic curve is fitted to all points except 5 and 6, which were measured under atypical flow conditions (5 under fast, shallow flow, 6 in deep, stagnant water). Reduced major axis regression, $R = 0.21\Omega^2$, $r^2 = 0.994$ (linearized).

$$\frac{E}{I} = \frac{\delta_I - \delta_L}{\delta_E - \delta_L},$$

where the isotopic composition δ_E of the evaporative flux can be estimated using the linear resistance model of Craig & Gordon (1965):

$$\delta_E = \frac{(1 + 10^{-3}\varepsilon^*)\delta_L - h\delta_A - \varepsilon^* - \varepsilon_K}{1 - h + 10^{-3}\varepsilon_K}.$$

The relative humidity h was set to 0.85, based on historical records for Spitzbergen in August. The parameter ε*, representing equilibrium fractionation, was estimated using the empirical relation of Horita & Wesolowski (1994):

$$\varepsilon^* = -7.685 + 6.7123\left(\frac{10^3}{T}\right) - 1.6664\left(\frac{10^6}{T^2}\right) + 0.3504\left(\frac{10^9}{T^3}\right)$$

with $T = 294$ K.

The value ε_K represents kinetic effects, and was estimated using the relation of Gonfiantini (1986):

$$\varepsilon_K = 14.2(1 - h).$$

The isotopic composition of ambient moisture δ_A was not measured, but was estimated from the composition of rain water as $\delta_A = \delta_P - \varepsilon$* (but see Gibson *et al.* 1999 for problems with this approach). The IAEA GNIP database reports $\delta_P = -12.8‰$ relative to SMOW in nearby Ny Alesund in August 2000. Using the oxygen isotopic composition of sample 0 (source) as the inflow value, and sample 10 (uppermost, stagnant pool) as the locality L, this method gives an evaporation of 1.2%. A δ_P value of −15.1, as measured by us in the presumably meteorically sourced cold spring K1 close to the Troll springs, gives an evaporation of 1.6%. Both these values are somewhat lower than the evaporation calculated above using Cl as a conservative marker. The isotopic estimate of evaporation is very rough, mainly because of the sensitivity to the value of δ_A that was not measured, but still indicates that evaporation is more than sufficient as a mechanism to explain the trend in oxygen isotopic composition, because the observed reduction in light oxygen is not even as large as expected from the evaporation calculated from chloride concentrations.

Bioeffects

Bromide does not follow the distribution pattern of chloride, and the Br concentration decreases downstream (Fig. 5). This loss of bromide is unlikely to be due to inorganic precipitation in the travertine, and is possibly an effect of organic uptake. Considerable assimilation of bromide by green plants is now well documented (Whitmer *et al.* 2000), and the photosynthetic purple bacteria that are found throughout the Troll 3A system (A. Steele, personal communication) may be a possible bromide sink. Organic uptake is furthermore supported by the positive correlation between Br and SO_4.

Nitrate concentrations are low compared with typical natural levels, but highest in a region around the inlet of the uppermost pool (sample 15), where there is lush growth of algal and bacterial filaments. Nitrate levels are comparatively low in the source itself and in the most distal pools.

The effect of biota on sinter formation is supported by the microscopic evidence showing that only calcite mats that precipitate at the sinter edges are full of micro-organisms (Fig. 9E,F). Their presence in the waters themselves is obvious but presumably they do not influence calcite precipitation in the waters until after colonizing the formed sinter edge.

CONCLUSION

The measured downstream trends in water chemistry at the Troll 3A spring are consistent with a model of calcite precipitation driven by progressive loss of CO_2, most likely due to degassing. Evaporation is also an important control on water chemistry. Nitrate and bromide concentrations may be controlled by biological activity. The main precipitate is calcite, and a maximum precipitation rate of around 2 mm year^{-1} was measured. This rate is controlled in part by calcium carbonate saturation, which in turn is controlled by CO_2 levels, and partly by water depth and flow rate.

ACKNOWLEDGEMENTS

We acknowledge field and infrastructure support from PGP for the AMASE 2003 expedition, and specifically Hans Amundsen without whom this work would not have been possible. Solution analyses have been supported in Leeds by the JIF-funded ICP-MS facility.

REFERENCES

Banks D, Siewers U, Sletten RS, Haldorsen S, Dale B, Heim M, Swensen B (1997) *The Thermal Springs of Bockfjord, Svalbard – Hydrogeochemical Data Report*, 97.183. Geological Survey of Norway, Trondheim.

Banks D, Sletten RS, Haldorsen S, Dale B, Heim M, Swensen B (1998) The thermal springs of Bockfjord, Svalbard: occurrence and major ion hydrochemistry. *Geothermics*, **27**, 445–67.

Buhmann D, Dreybrodt W (1985) The kinetics of calcite dissolution and precipitation in geologically relevant situations of karst areas. 1. Open system. *Chemical Geology*, **48**, 189–211.

Craig H, Gordon LI (1965) Deuterium and Oxygen-18 variations in the ocean and marine atmosphere. In: *Stable Isotopes in Oceanographic Studies and Paleo-Temperatures*, (ed Tongiorgi E), pp. 9–130. Laboratorio di Geologia Nucleare, Pisa.

Dreybrodt W, Buhmann D, Michaelis J, Usdowski E (1992) Geochemically controlled calcite precipitation by CO_2 outgassing: field measurements of precipitation rates in comparison to theoretical predictions. *Chemical Geology*, **97**, 285–94.

Fouke BW, Farmer JD, Des Marais DJ, Pratt L, Sturchio NC, Burns PC, Discipulo MK (2000) Depositional facies and aqueous-solid geochemistry of travertine-depositing hot springs (Angel Terrace, Mammoth hot springs, Yellowstone national park, USA). *Journal of Sedimentary Research*, **70**, 565–85.

Gibson JJ, Edwards TWD, Prowse TD (1999) Pan-derived isotopic composition of atmospheric water vapour and its variability in northern Canada. *Journal of Hydrology*, **217**, 55–74.

Gonfiantini R (1986) Environmental isotopes in lake studies. In: *Handbook of Environmental Isotope Geochemistry*, Vol. 3. (eds. Fritz P, Fontes JC), pp. 113–68. Elsevier, New York.

Hoel A, Holtedahl O (1911) Les nappes de lave, les volcans et les sources thermales dans les environs de la baie Wood au Spitsberg. *Videnskapsselskapets skrifter (Christiania), I. Matematisk-naturvidenskabelig klasse*, **8**, 37.

Horita J, Wesolowski D (1994) Liquid-vapour fractionation of oxygen and hydrogen isotopes of water from the freezing to the critical temperature. *Geochimica et Cosmochimica Acta*, **58**, 3425–37.

Isaksson E, Pohjola V, Jauhiainen T, Moore J, Pinglot J-F, Vaikmäe R, van de Wal RSW, Hagen J-O, Ivask J, Karlöf L, Martma T, Meijer HAJ, Mulvaney R, Thomassen MPA, Van den Broeke M (2001) A new ice core record from Lomonosovfonna, Svalbard: viewing the data between 1920–1997 in relation to present climate and environmental conditions. *Journal of Glaciology*, **47**, 335–45.

Lu G, Zheng C, Donahoe RJ, Berry Lyons W (2000) Controlling processes in a $CaCO_3$ precipitating stream in Huanglong Natural Scenic District, Sichuan, China. *Journal of Hydrology*, **230**, 34–54.

Parkhurst DL, Appelo CAJ (1999) *User's Guide to PHREEQC (version 2) – A Computer Program for Speciation, Batch-reaction, One-dimensional Transport, and Inverse Geochemical Calculations.* Water-Resources Investigations Report 99-459, USGS, Denver, Colorado.

Poage MA, Chamberlain CP (2001) Empirical relationships between elevation and the stable isotope composition of precipitation and surface waters: Considerations for studies of paleoelevation change. *American Journal of Science*, **301**, 1–15.

Skjelkvåle BL, Amundsen HEF, O'Reilly SY, Griffin WL, Gjelsvik T (1989) A primitive alkali basaltic stratovolcano and associated eruptive centres, Northwestern Spitsbergen: volcanology and tectonic significance. *Journal of Volcanology and Geothermal Research*, **37**, 1–9.

Tesoriero AJ, Pankow JF (1996) Solid solution partitioning of Sr^{2+}, Ba^{2+} and Cd^{2+} to calcite. *Geochimica et Cosmochimica Acta*, **60**, 1053–63.

Watanabe O, Motoyama H, Igarishi M, Kamiyama K, Matoba S, Goto-Azuma K, Narita H, Kameda T (2001) Studies on climatic and environmental changes during the last few hundred years using ice cores from various sites in Nordaustlandet, Svalbard. *Memoirs of National Institute of Polar Research, Special Issue*, **54**, 227–42.

Whitmer S, Baker L, Wass R (2000) Loss of bromide in a wetland tracer experiment. *Journal of Environmental Quality*, **29**, 2043–5.

Zaihua L, Svensson U, Dreybrodt W, Daoxian Y, Buhmann D (1995) Hydrodynamic control of inorganic calcite precipitation in Huanglong Ravine, China: field measurements and theoretical prediction of deposition rates. *Geochimica et Cosmochimica Acta*, **59**, 3087–97.